Measurement of H^N-H^α J couplings in calcium-free calmodulin using new 2D and 3D water-flip-back methods

Hitoshi Kuboniwa, Stephan Grzesiek, Frank Delaglio and Ad Bax

*Laboratory of Chemical Physics, National Institute of Diabetes and Digestive and Kidney Diseases,
National Institutes of Health, Bethesda, MD 20892-0520, U.S.A.*

SUMMARY

Two new methods are described for the measurement of three-bond $J_{H_N H\alpha}$ couplings in proteins isotopically enriched with ^{15}N. Both methods leave the water magnetization in an unsaturated state, parallel to the z-axis, and therefore offer significant enhancements in sensitivity for rapidly exchanging backbone amide protons. The J couplings can be measured either from a set of constant-time 2D ^1H-^{15}N HMQC spectra, which are modulated in intensity by $J_{H_N H\alpha}$, or from a water-flip-back version of the 3D HNHA experiment. The method is demonstrated for a sample of calcium-free calmodulin. Residues Lys^{75}-Asp^{80} have $J_{H_N H\alpha}$ values in the 6–7 Hz range, suggesting that a break in the 'central helix' occurs at the same position as previously observed in solution NMR studies of Ca^{2+}-ligated calmodulin.

Numerous methods have been proposed in recent years for measurement of homonuclear three-bond $J_{H_N H\alpha}$ coupling constants in proteins. These include fitting procedures of antiphase doublets in COSY-type spectra (Ludvigsen et al., 1991; Smith et al., 1991), measurement of J splittings in resolution-enhanced ^{15}N-^1H HMQC spectra (Kay et al., 1989), E.COSY-type triple-resonance experiments on proteins uniformly enriched with both ^{13}C and ^{15}N (Montelione and Wagner, 1989; Wagner et al., 1991; Seip et al., 1994), nonlinear fitting of J-modulated ^{15}N-^1H HSQC spectra (Billeter et al., 1992), and quantitative evaluation of the cross peak–diagonal peak intensity ratio in a ^{15}N-separated 3D HNHA experiment (Vuister and Bax, 1993). Although many of these experiments do not require presaturation of the H_2O resonance, this resonance invariably ends up in a saturated 'scrambled' state because either the inhomogeneity of the rf field (Messerle et al., 1989) or of the B_0 field (John et al., 1991; Kay et al., 1992) is used to dephase its magnetization. H_2O has a much longer T_1 value than the protein backbone amide protons and therefore remains in a semisaturated state when the repetition rate of the pulse sequence is optimized for protein resonances. In many of the common heteronuclear experiments one can avoid saturation of H_2O, thereby improving the sensitivity for rapidly exchanging amide protons in these so-called water-flip-back experiments by more than twofold compared to analogous water-scrambling

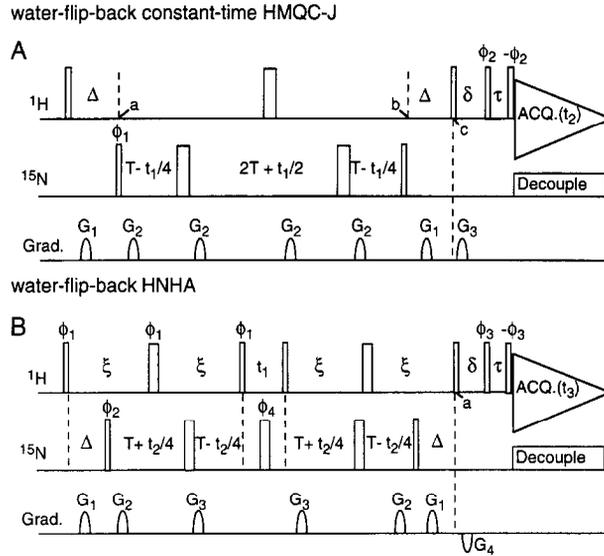water-flip-back constant-time HMQC-J

water-flip-back HNHA

Fig. 1. Pulse schemes of (A) the water-flip-back 2D CT-HMQC-J experiment and (B) the water-flip-back 3D HNHA experiment. Narrow and wide pulses correspond to 90° and 180° flip angles, respectively, and were applied along the x-axis unless indicated otherwise. For scheme (A), the following eight-step phase cycle was used: $\phi_1 =$ x,−x; $\phi_2 =$ 2x,2y,2(−x),2(−y); receiver = x,−x,y,−y,−x,x,−y,y. Quadrature detection in t_1 was obtained with the States-TPPI method (Marion et al., 1989), incrementing phase ϕ_1. Delays are: $\Delta =$ 5.3 ms; $\delta =$ 2 ms; $\tau =$ 90 μs; T was varied from 8.6 to 32.35 ms in separate 2D experiments. Gradients: $G_{1,2,3} =$ 0.3, 0.45, 0.5 ms. For obtaining zero linear phase gradient in the F_1 dimension, the first t_1 duration should be set to $4\tau_{90N}/\pi$, where τ_{90N} is the duration of the 90° ^{15}N pulse. For scheme (B), the following eight-step phase cycle was used: $\phi_1 =$ 2x,2(−x); $\phi_2 =$ x; $\phi_3 =$ 4x,4y; $\phi_4 =$ x,y; receiver = x,2(−x),x,y,2(−y),y. Quadrature detection was obtained using States-TPPI on ϕ_1 for the t_1 dimension, and on ϕ_2 for the t_2 dimension. Delay durations: $\xi =$ 13.4 ms; $\Delta =$ 5.3 ms; $\delta =$ 2 ms; $\tau =$ 90 μs. Gradients: $G_{1,2,3,4} =$ 0.3, 0.45, 0.75, 0.5 ms. G_4 has negative polarity. All gradients are sine-bell shaped, with a gradient strength of 25 G/cm at their midpoint. For both experiments the carrier was positioned at the H_2O frequency.

versions (Roy et al., 1984; Campbell-Burk et al., 1991; Grzesiek and Bax, 1993; Kay et al., 1994; Stonehouse et al., 1994). Here, we present two experiments for measurement of $J_{HNH\alpha}$ which both utilize the water-flip-back concept to avoid water excitation, without requiring selective H_2O pulses. The first experiment is analogous to the J-modulated HSQC experiment of Neri et al. (1990); the second is a variation on the recently proposed 3D HNHA experiment for which only a water presaturation sequence had been proposed (Vuister and Bax, 1993).

Pulse sequences for the new experiments, which we refer to as water-flip-back constant-time (CT) HMQC-J and water-flip-back 3D HNHA, are shown in Fig. 1. Both experiments benefit from the longer T_2 value of ^{1}H-^{15}N multiple-quantum coherence relative to that of H^N single-quantum coherence (Bax et al., 1989), as the magnetization prior to detection exists as multiple-quantum coherence for all but 10 ms.

In the constant-time HMQC-J experiment, H^N-H^α J modulation is present for a time 4T + 2Δ, and heteronuclear two-spin (^{1}H^N-^{15}N) coherence is present between time points a and b, which interval comprises the constant-time evolution period 4T. At time point c, the in-phase component of the transverse H^N magnetization is stored along the z-axis by a 90°_x pulse. H_2O magnetization is also returned to the +z-axis by this pulse. Note that the effects of H_2O radiation damping during the 4T + 2Δ period are minimized by the application of pulsed field gradients G_1 (and also

by G_2). These gradients are made sufficiently weak so that diffusion of H_2O during the period $4T + 2\Delta$ does not significantly affect the refocusing of its magnetization at time c. After application of gradient pulse G_3, the in-phase H_N magnetization is monitored by a conventional jump-and-return $90_{\phi 2}$-τ-$90_{-\phi 2}$ pulse pair (Plateau and Gueron, 1982), or by any other type of excitation scheme that yields adequate H_2O suppression. Temporarily ignoring the effect of H^α spin flips during the $J_{H^N H^\alpha}$ dephasing period, the peak height of the observed ^1H-^{15}N correlation is described by

$$I = C \ N_1 \ \cos[\pi J_{HH}(4T + 2\Delta)] \ \exp(-4T/T_{2,MQ}) \tag{1}$$

where C is a constant which also incorporates the effect of transverse relaxation during the two Δ-periods and $T_{2,MQ}$ is the transverse relaxation rate of the $^1H^N$-^{15}N two-spin coherence. N_1 is the number of t_1 increments in the constant-time dimension. The resolution that can be obtained in the t_1 dimension is limited by the duration of the constant-time evolution period and we therefore prefer to use the maximum number of t_1 increments that can be accommodated within the $4T$ period. Note that the integrated signal intensity is independent of N_1, but as the F_1 line width is inversely proportional to N_1, the peak height I increases linearly with N_1.

As pointed out by Harbison (1993), H^α spin flips can significantly affect the apparent value of $J_{H^N H^\alpha}$. In the HMQC-J experiment, the effect of the H^α selective T_1 ($T_{1,\alpha}$) on the spin state of H^α (A_z) is easily accounted for when considering the time evolution of the in-phase (I_y) and the antiphase ($2I_xA_z$) H^N magnetization, which to a good approximation may be described by

$$\frac{d}{dt} \begin{pmatrix} I_y \\ 2I_xA_z \end{pmatrix} = \begin{pmatrix} -1/T_{2,MQ} & -\pi J_{HH} \\ \pi J_{HH} & -1/T_{2,MQ} -1/T_{1,\alpha} \end{pmatrix} \begin{pmatrix} I_y \\ 2I_xA_z \end{pmatrix} \tag{2}$$

After integration one obtains:

$$I_y(t) = I_y(0) \ \exp[-t/T_{2,MQ} - t/(2T_{1,\alpha})] \ \{\exp(i\omega t/2) + \exp(-i\omega t/2) + [\exp(i\omega t/2) - \exp(-i\omega t/2)]/(iT_{1,\alpha}\omega)\}/2 \tag{3}$$

with $\omega = \sqrt{4\pi^2 J_{HH}^2 - 1/(T_{1,\alpha})^2}$.

For $J_{HH} > 1/(2\pi T_{1,\alpha})$, Eq. 3 can be rewritten as:

$$I_y(t) = I_y(0) \ N_1 \exp[-t/T_{2,MQ} - t/(2T_{1,\alpha})] \ \{\cos(\pi J^r t) + \sin(\pi J^r t)/(2\pi J^r T_{1,\alpha})\} \tag{4}$$

with $J^r = \sqrt{J_{HH}^2 - 1/(2\pi T_{1,\alpha})^2}$, where the factor N_1 from Eq. 1 has been included again. Equation 4 shows the apparent reduction in the modulation frequency, J^r, caused by finite values of $T_{1,\alpha}$. The value for $1/T_{1,\alpha}$ is dominated by ^1H-^1H spin flips and therefore depends nearly linearly on the rotational correlation time, τ_0, of the protein.

The pulse scheme of Fig. 1B is virtually identical to the original HNHA scheme, except for the last three ^1H pulses. The phase of the 90° pulse applied at time point a differs by 90° from that in the original pulse scheme and rotates both the H_2O and the in-phase H^N magnetization back to the z-axis. After a short delay, δ, which contains field gradient G_4, a $90_{\phi 3}$-τ-$90_{-\phi 3}$ pulse pair is used to 'read' the z magnetization without a net perturbation of the water magnetization. A detailed
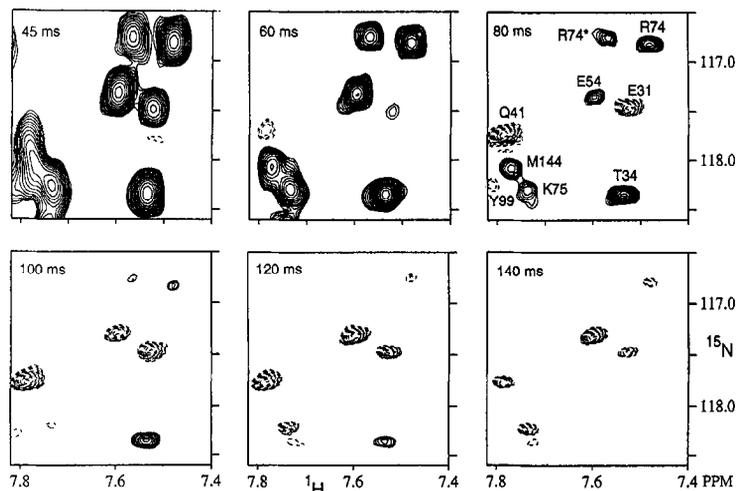
Fig. 2. Small sections of the CT-HMQC-J spectra of Ca^{2+}-free calmodulin, recorded with the pulse scheme of Fig. 1A, using dephasing periods ($4T + 2\Delta$) of 45, 60, 80, 100, 120 and 140 ms. Each spectrum results from 64 scans per complex t_1 increment and the total recording time for the six spectra was 12 h. The acquired data matrices contain 38, 56, 81, 106, 131 and 156 complex data points in the t_1 dimension. For all six spectra mirror-image linear prediction (using 16 coefficients) was used to double the duration of the t_1 time domain (Zhu and Bax, 1990), prior to apodization with a squared cosine-bell window function. All spectra were zero-filled to yield digital resolutions of 2.4 (F_1) and 9.0 (F_2) Hz.

analysis of the magnetization transfer pathways during this pulse scheme has been presented previously (supplementary material to Vuister and Bax, 1993) and will not be repeated here. The 3D HNHA spectrum yields diagonal peaks at $(F_1,F_2,F_3) = (\omega_{HN},\omega_N,\omega_{HN})$, and cross peaks at $(F_1,F_2,F_3) = (\omega_{H\alpha},\omega_N,\omega_{HN})$. Provided that the t_1 acquisition period is much shorter than $1/J_{H\alpha H\beta}$, the diagonal and cross peaks have identical line shapes. If this condition is not met, integrated intensities of the cross peak (I_X) and of the diagonal peak (I_D) need to be compared. The intensity ratio is related in a very simple manner to the size of $J_{HNH\alpha}$:

$$I_X/I_D = -\tan^2(2\pi\xi\, J_{HNH\alpha}) \tag{5}$$

If the $J_{HNH\alpha}$ de-/rephasing periods, 2ξ, are short compared to $1/(2J_{HNH\alpha})$, H^α spin flips during these periods cause a reduction in the $J_{HNH\alpha}$ value derived using Eq. 5 by a uniform factor (Vuister and Bax, 1993) relative to the true value. For a $T_{1\alpha}$ value of 100 ms, this factor was estimated to be 0.9.

The experiments discussed above are demonstrated for a sample of calcium-free *Xenopus* calmodulin, 5 mg in a 200 μl Shigemi microcell (1.5 mM), 1 mM EDTA, 0.1 M KCl, pH 6.5, 23 °C. Experiments were carried out on a Bruker AMX-600 spectrometer, using a triple-resonance probehead equipped with a self-shielded z gradient.

Figure 2 shows small regions of six 2D CT-HMQC-J spectra, recorded for different $J_{HNH\alpha}$ dephasing periods. Resolution in the F_1 dimension was enhanced for all six spectra by mirror-image linear prediction (Zhu and Bax, 1990), but due to the conservative digital filtering, the predicted part of the time domain actually contributes relatively little (~19%) to the peak intensity. A reasonable estimate for $J_{HNH\alpha}$ can be obtained from the dephasing time duration where the signal intensity changes sign, which to a first approximation corresponds to $1/2J_{HNH\alpha}$. More

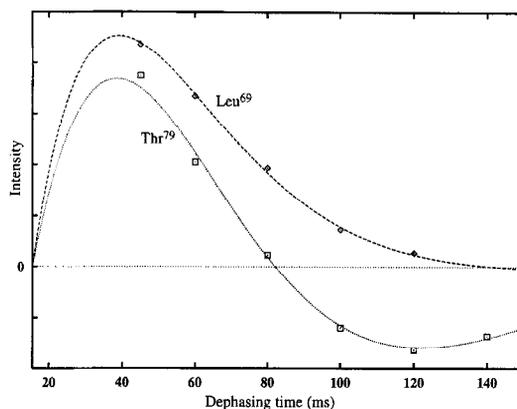Fig. 3. Best fits to Eq. 4 for the peak heights of residues Leu[69] and Thr[79] in the six CT-HMQC-J spectra.

accurate values can be obtained when fitting the intensities to Eq. 4. Figure 3 shows such fits for Leu[69] and Thr[79], assuming a $T_{1,\alpha}$ value of 100 ms. This value is based on ^{15}N relaxation measurements which indicate that the rotational correlation time is very similar to that of staphylococcal nuclease ($\tau_c \sim 8$ ns), for which a $T_{1,\alpha}$ of ca. 100 ms has previously been measured for the H$^\alpha$ protons in a selectively labeled [13]C$^\alpha$-Ala sample (L.K. Nicholson and D.A. Torchia, unpublished results). Values obtained for residues Phe[68]-Glu[84] are reported in Table 1. As can be seen from this table, residues with small J values or with short decay constants on average have larger uncertainties for $J_{H^N H^\alpha}$. In practice, $J_{H^N H^\alpha}$ values measured from the HMQC-J spectra are most accurate if the modulation pattern shows at least one zero-crossing.

TABLE 1
$J_{H^N H^\alpha}$ VALUES FOR RESIDUES Phe[68]-Glu[84] IN Ca^{2+}-FREE CALMODULIN^a

Residue	$J_{H^N H^\alpha}$ (HNHA)	$J_{H^N H^\alpha}$ (HMCQ-J)	$T_{2,MQ}$ (ms)^b	Residue	$J_{H^N H^\alpha}$ (HNHA)	$J_{H^N H^\alpha}$ (HMCQ-J)	$T_{2,MQ}$ (ms)^b
Phe[68]	5.4 ± 0.3	5.3 ± 0.4	31 ± 6	Lys[77]	c	6.4 ± 0.0	35 ± 1
Thr[70]	4.4 ± 0.2	5.0 ± 0.4	44 ± 12	Asp[78]	c	6.9 ± 0.0	40 ± 1
Met[71]	4.9 ± 0.2	4.0 ± 1.8	25 ± 14	Thr[79]	6.8 ± 0.2	7.1 ± 0.0	44 ± 1
Met[72]	c	5.3 ± 0.3	27 ± 4	Asp[80]	6.7 ± 0.2	7.0 ± 0.0	47 ± 2
Ala[73]	3.8 ± 0.2	4.9 ± 0.2	40 ± 5	Ser[81]	5.6 ± 0.2	5.8 ± 0.0	37 ± 2
Arg[74]	4.8 ± 0.2	5.5 ± 0.1	43 ± 3	Glu[82]	c	5.4 ± 0.1	45 ± 2
Lys[75]	6.1 ± 0.2	6.5 ± 0.1	36 ± 1	Glu[83]	c	5.4 ± 0.1	30 ± 1
Met[76]	6.5 ± 0.2	6.6 ± 0.1	39 ± 1	Glu[84]	4.7 ± 0.2	5.7 ± 0.2	45 ± 7

^{a} For a 1.5 mM sample concentration of U-[15]N *Xenopus* calmodulin in 95% H$_2$O/5% D$_2$O, 0.1 M KCl, pH 6.5, 1 mM EDTA, 23 °C, assuming a uniformly selective T_1 for the H$^\alpha$ protons of 100 ms. The calmodulin lacks posttranslational acetylation at the N-terminus and trimethylation of Lys[115]. Approximately a 30% fraction of the protein is formylated at the N-terminus. J values are in hertz. Uncertainties in J values derived from CT-HMQC-J spectra are based on multiple fits of Eq. 4, randomly adding a 5% uncertainty to the peak intensities. Uncertainties in HNHA-derived J values are also based on an estimated 5% error in the diagonal and cross-peak intensities, except for weak cross peaks where the error was estimated to be identical to the rms noise in the 3D spectrum.
^{b} Value obtained from fitting Eq. 4 to the peak heights.
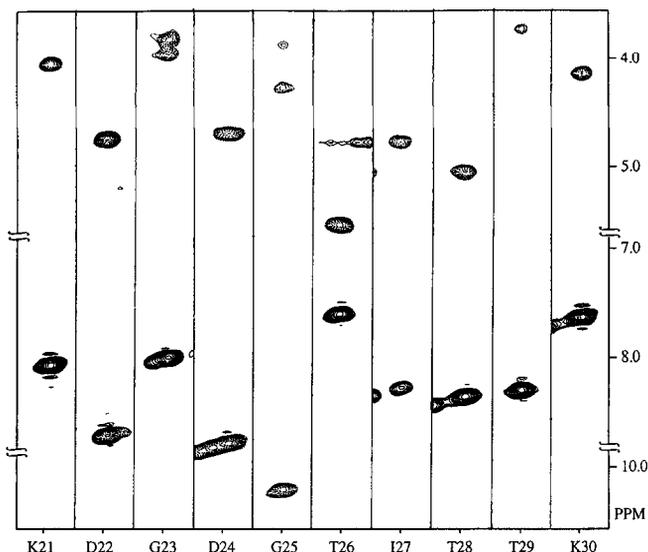^{c} No reliable measurement of diagonal peak intensity was possible due to partial overlap.

Fig. 4. F_1 strips taken from the 3D HNHA spectrum of calcium-free calmodulin for residues Lys^{21}-Lys^{30}. The 3D spectrum results from a $70^* \times 47^* \times 512^*$ data matrix, with acquisition times of 15.4 (t_1), 38 (t_2) and 55 (t_3) ms. Acquired data were apodized with a $65°$-shifted squared sine-bell in the t_3 dimension, truncated at 10% ($\sin^2 162°$) at the end of the FID, and with a $68°$-shifted sine-bell in the t_1 dimension, also truncated at 10% (at sin $174°$). Truncation at the end of the sine-bell is used as a compromise between maximizing spectral resolution (and sensitivity) and minimizing truncation artifacts. The t_2 (^{15}N) time domain data has been extended to 83^* data points by mirror-image linear prediction, prior to apodization with a squared cosine-bell and zero-filling to 128^*. Digital resolutions in the final 3D spectrum were 17.7 (F_1), 9.6 (F_2) and 4.5 (F_3) Hz. Total acquisition time was 32 h.

Figure 4 shows F_1 strips taken from the water-flip-back HNHA 3D spectrum, recorded with J de-/rephasing times of 26.8 ms, for residues Lys^{21}-Lys^{30}. The optimal choice for the duration of 2ξ is a compromise between optimizing resolution in the ^{15}N dimension, which requires a long value for 2ξ, and minimizing the effects of H^α spin flips during these periods by keeping 2ξ short. H^N-H^α cross-peak intensities depend strongly on the size of $J_{H^N H^\alpha}$ and small J values yield weak cross peaks. The intensity of these weak cross peaks is maximized by choosing $2\xi \approx$ $[(2\xi - \Delta)T_{2,MQ} + \Delta T_{2,HN}]/2\xi$, where $T_{2,MQ}$ is the decay constant of the ^1H-^{15}N heteronuclear two-spin coherence and $T_{2,HN}$ is the amide proton T_2 value. For the 26.8-ms value for 2ξ used in the present study, virtually all backbone amides which are not broadened by slow conformational exchange yield observable H^N-H^α cross peaks. However, quantitative measurement of $J_{H^N H^\alpha}$ from such a spectrum requires that the intensity of the diagonal resonance can be measured reliably, i.e., that it is well resolved. The resolution for the diagonal $^1H^N$-^{15}N-$^1H^N$ resonances is the same as in a 2D ^1H-^{15}N constant-time HSQC, recorded with a 38-ms ^{15}N evolution period. In the 3D HNHA spectrum of Ca^{2+}-free calmodulin, the diagonal peak intensities can be measured for 98 out of the 132 residues with observable H^N-H^α cross peaks. Again assuming an H^α-selective T_1 value of 100 ms, the $J_{H^N H^\alpha}$ values derived from Eq. 5 need to be multiplied by a factor of 1.11 to account for H^α spin flips (Vuister and Bax, 1993).

Besides the H^N-H^α J connectivity information available from the 3D HNHA spectrum, an additional advantage over the CT-HMQC-J experiment is found for glycines. Provided that the two geminal glycine H^α resonances differ in chemical shift, the individual $J_{H^N H^\alpha}$ values can be
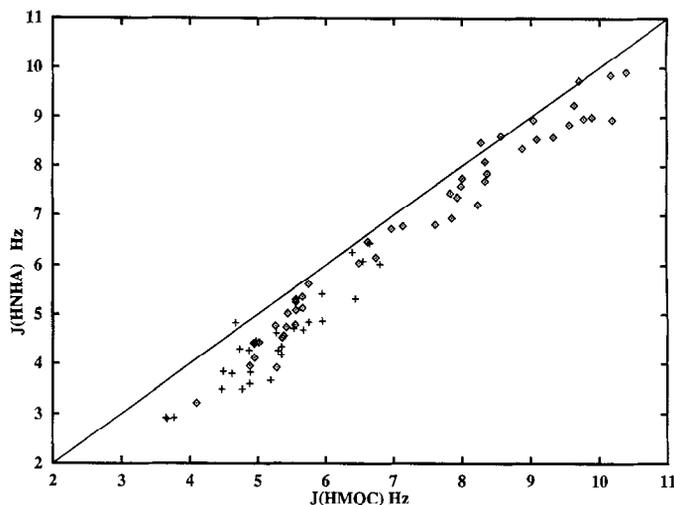
Fig. 5. Comparison of J values obtained from the HNHA experiment with those of the CT-HMQC-J experiment. Residues which do not exhibit a zero-crossing in the CT-HMQC-J experiment are denoted '+'. Only J values with errors less than 1 Hz, as determined by the procedure described in the footnote to Table 1, are included in the comparison. On average, CT-HMQC-J-derived values are 0.63 Hz larger than HNHA-derived J values.

measured separately. Although the modulation pattern for glycine amides in the CT-HMQC-J experiment can be fit to a product of two cosine functions, in practice such a fit to two frequencies only yields reliable results if the intensity modulation pattern shows at least two zero-crossings, which is not the case for any of the glycines in calmodulin.

Figure 5 compares the values measured by the CT-HMQC-J experiment with the HNHA values and shows that, on average, the CT-HMQC-J values are larger than J values derived from the HNHA spectrum. The rms difference between the two measured sets is 0.72 Hz and the average difference is 0.63 Hz. After adding 0.63 Hz to the HNHA-derived J values, the rms difference reduces to 0.36 Hz. Previously, HNHA J couplings measured for staphylococcal nuclease showed no such systematic difference when compared to splittings measured from an HMQC-J experiment (Vuister and Bax, 1993). However, in this comparison the HNHA-derived J values had been corrected for the finite lifetime of the H^α spin state, whereas the HMQC-J values had not. Such a correction results in an increase of $J_{HN H\alpha}$ and if both data sets had been corrected, the HNHA-derived J couplings, on average, would also be smaller by a few tenths of a hertz. This small but systematic underestimate in the quantitative J correlation experiments has also been noted for heteronuclear J measurements and has been ascribed to rf inhomogeneity (Zhu and Bax, 1993). In the present case, if the ^1H pulses immediately preceding and following the t_1 evolution period deviate from 90°, this affects the diagonal and cross-peak intensities differently. A simple product-operator calculation indicates that the cross-peak intensity is attenuated by $sin^4\alpha$, where α is the effective flip angle of the nominal 90° ^1H pulse, whereas the diagonal resonance is attenuated by $tan^2(2\pi J\xi)sin^4\alpha$. This indicates that the effect of rf inhomogeneity on the derived J coupling should disappear when $tan^2(2\pi J\xi) = 1$ (J ≈ 9 Hz). Although the systematic difference between the two sets of J couplings decreases for larger J values, particularly when expressed as a fraction of the measured value, a small systematic difference remains even for the larger J couplings. The source of this residual anomaly has not yet been identified.

The $J_{H_NH\alpha}$ values reported for residues Phe[68]-Glu[84] are compatible with an α-helical conformation for this region of the protein, except for residues Lys[75]-Thr[80] which exhibit $J_{H_NH\alpha}$ values in the 6–7 Hz range. As was found for calcium-bound calmodulin (Spera et al., 1991; Barbato et al., 1992), the amide protons of these latter residues exchange rapidly with solvent and ^{15}N relaxation experiments show an increase in internal dynamics (H. Kuboniwa, unpublished results). The J couplings combined with the hydrogen exchange and ^{15}N relaxation data therefore suggest a high degree of flexibility in this region. In the X-ray crystal structure of Ca^{2+}-ligated calmodulin, these residues constitute the fully solvent-exposed part of a so-called 'central helix', which connects the globular N- and C-terminal domains. For Ca^{2+}-free calmodulin, we find that slow conformational exchange causes severe line broadening for most of the C-terminal residues of this 'central helix' (Ile[85]-Phe[92]) and only a few $J_{H_NH\alpha}$ values could be measured in the latter region.

ACKNOWLEDGEMENTS

REFERENCES

Barbato, G., Ikura, M., Kay, L.E. and Bax, A. (1992) *Biochemistry*, **31**, 5269–5278.

Bax, A., Kay, L.E., Sparks, S.W. and Torchia, D.A. (1989) *J. Am. Chem. Soc.*, **111**, 408–409.

Billeter, M., Neri, D., Otting, G., Qian, Y.Q. and Wüthrich, K. (1992) *J. Biomol. NMR*, **2**, 257–274.

Campbell-Burk, S., Domaille, P. and Mueller, L. (1991) *J. Magn. Reson.*, **93**, 171–177.

Grzesiek, S. and Bax, A. (1993) *J. Am. Chem. Soc.*, **115**, 12593–12594.

Harbison, G. (1993) *J. Am. Chem. Soc.*, **115**, 3026–3027.

John, B.K., Plant, D., Heald, S.H. and Hurd, R.E. (1991) *J. Magn. Reson.*, **94**, 664–669.

Kay, L.E., Brooks, B., Sparks, S.W., Torchia, D.A. and Bax, A. (1989) *J. Am. Chem. Soc.*, **111**, 5488–5490.

Kay, L.E., Keifer, P. and Saarinen, T. (1992) *J. Am. Chem. Soc.*, **114**, 10663–10665.

Kay, L.E., Xu, G.Y. and Yamazaki, T. (1994) *J. Magn. Reson. Ser. A*, **109**, 129–133.

Ludvigsen, S., Andersen, K.V. and Poulsen, F.M. (1991) *J. Mol. Biol.*, **217**, 731–736.

Marion, D., Ikura, M., Tschudin, R. and Bax, A. (1989) *J. Magn. Reson.*, **85**, 393–399.

Messerle, B.A., Wider, G., Otting, G., Weber, C. and Wüthrich, K. (1989) *J. Magn. Reson.*, **85**, 608–613.

Montelione, G.T. and Wagner, G. (1989) *J. Am. Chem. Soc.*, **111**, 5474–5475.

Neri, D., Otting, G. and Wüthrich, K. (1990) *J. Am. Chem. Soc.*, **112**, 3663–3665.

Plateau, P. and Gueron, M. (1982) *J. Am. Chem. Soc.*, **104**, 7310–7311.

Roy, S., Papastavros, M., Sanchez, V. and Redfield, A.G. (1984) *Biochemistry*, **23**, 4395–4400.

Seip, S., Balbach, J. and Kessler, H. (1994) *J. Magn. Reson. Ser. B*, **104**, 172–179.

Smith, L.J., Sutcliffe, M.J., Redfield, C. and Dobson, C.M. (1991) *Biochemistry*, **30**, 986–996.

Spera, S., Ikura, M. and Bax, A. (1991) *J. Biomol. NMR*, **1**, 155–165.

Stonehouse, J., Shaw, G.L., Keeler, J. and Laue, E.D. (1994) *J. Magn. Reson. Ser. A*, **107**, 178–184.

Vuister, G.W. and Bax, A. (1993) *J. Am. Chem. Soc.*, **115**, 7772–7777.

Wagner, G., Schmieder, P. and Thanabal, V. (1991) *J. Magn. Reson.*, **93**, 436–440.

Zhu, G. and Bax, A. (1990) *J. Magn. Reson.*, **90**, 405–410.

Zhu, G. and Bax, A. (1993) *J. Magn. Reson. Ser. A*, **104**, 353–357.